Article

Not peer-reviewed version

Beta-Cyclodextrin Molecules (β-CD) Modified PVDF Membranes to Remove Multi-Ionic Dye Solutions using Steric, Inclusion, and Dielectric Exclusion

Wadha Alrashedi , Hafedh Ben KOCHKAR * , Ismail Ercan

Posted Date: 18 April 2024

doi: 10.20944/preprints202404.1247.v1

Keywords: β-cyclodextrin; hydrophilicity; PVDF membrane; Dye separation; dielectric exclusion

 doi:10.20944/preprints202404.1247.v1

Article

Beta-Cyclodextrin Molecules (β-CD) Modified PVDF Membranes to Remove Multi-Ionic Dye Solutions using Steric, Inclusion, and Dielectric Exclusion

Wadha Alrashedi [1,2], Hafedh Kochkar [1,2,*] and Ismail Ercan [3]

[1] Department of Chemistry, College of Science, Imam Abdulrahman Bin Faisal University, P.O. Box 1982, 31441, Dammam and Saudi Arabia
[2] Basic & Applied Scientific Research Center, Imam Abdulrahman Bin Faisal University, P.O. Box 1982, 31441, Dammam, Saudi Arabia
[3] Department of Electrical and Electronics Engineering, Faculty of Engineering, Düzce University, 81010, Turkey
* Correspondence: hbkochkar@iau.edu.sa; Tel.: (00966557306180)

Abstract: In this study, we aim to evaluate how cyclodextrin molecules affect the hydrophilicity and selectivity of PVDF membrane. Herein, we prepared PVDF-PVP$_{(1-x)}$ β-CD$_x$ membranes, with x ranging from 0 to 1 wt%. The membranes were deeply characterized by means of X-ray diffraction (XRD), attenuated total reflectance infrared (ATR-IR), Raman spectroscopies, Thermal gravimetric analysis (TGA), Contact angle measurement (CA), scanning electron microscopy (SEM) and atomic force microscopy (AFM). The study unequivocally demonstrates the effectiveness of the addition of β-CD molecules on membranes' structural, morphological, and dielectric properties. Adding 0.25wt% β-CD enhanced hydrophilicity, with CA decreasing from 72.6° to 56° and roughness decreasing from 81 to 29 nm. The PVDF-PVP(1-x) β-CDx membranes were then fully characterized using electrochemical impedance spectroscopy (EIS) to determine their dielectric properties, which clearly showed that the presence of β-CD induced polarization of the membrane. The separation of various dyes with different sizes and charges was utilized. These dyes included methylene blue (MB, positive, 0.504 nm), methyl red (MR, neutral, 0.487 nm), rose Bengal (RB, negative, 0.588 nm), and brilliant blue (BB, negative, 0.798 nm). Based on our research, we found that the membrane's selectivity is determined by both exclusion factors (such as size and dielectric properties) and inclusion inside the β-CD cage. We found that using alpha-CD instead of beta-CD led to the disappearance of dye inclusion. These findings strongly suggest that β-CD molecules can be a viable solution for dye removal from wastewater.

Keywords: β-cyclodextrin; hydrophilicity; PVDF membrane; dye separation; dielectric exclusion

1. Introduction

Access to safe and clean water is crucial for maintaining good health as it plays a vital role in our life cycle [1]. Even though 97% of the earth's surface is covered with seawater [2], which is unsuitable for human consumption due to its high salt content, only 2.5% of the world's water is freshwater, with the remaining 2% being stored in glaciers and ice caps [3]. However, rapid urbanization and population growth have led to a water shortage and increased demand [4]. Discharging waste effluents from various sources such as industries, households, agriculture, and municipalities has limited the availability of clean water [5]. Such discharges are known to contain harmful substances such as dyes [6], heavy metals [7], and polycyclic aromatic hydrocarbons (PHAs) [8], which can be detrimental to marine ecosystems and human health. There are several effective techniques for removing organic materials from water, such as ozonation [9], adsorption [10], photocatalytic degradation [11], biosorption [12], chemical precipitation [13], and coagulation [14]. Nevertheless, membrane technology has emerged as a promising purifying and recycling water

 doi:10.20944/preprints202404.1247.v1

solution. With its advanced filtration capabilities, it has the potential to significantly improve water quality and address the growing concerns of water scarcity and pollution [15]. Membranes serve as selective barriers that allow desirable molecules to pass through while retaining undesirable ones [16]. Due to its high selectivity, low operating costs, ease of use, and low energy consumption, membrane separation technology has garnered more attention than traditional separation processes [17]. Effective and environmentally friendly water treatment methods include inorganic and organic membranes [18]. These membranes are made from a variety of polymers, such as cellulose acetate (CA) [19], chitosan [20], polyarylethersulfones (PAES) [21], polysulfone (PSF) [22], polycarbonate (PC) [23], and polyvinylidene fluoride (PVDF) [24]. PVDF is an extensively used semicrystalline polymer, which consists of repeating units of -CH_2CF_2-. It is highly valued for its ability to form membranes, excellent chemical resistance, and thermal stability [25]. PVDF is a versatile material that can be utilized to create various types of membrane systems, including microfiltration, ultrafiltration, and membrane distillation [26]. To dissolve PVDF, polar solvents such as N-methyl-2-pyrrolidone (NMP), N, N-dimethylacetamide (DMAc), and dimethylformamide (DMF) are commonly used[27]. There are several techniques available for preparing PVDF membranes, such as non-solvent-induced phase separation (NIPS), vapor-induced phase separation (VIPS)[28], and electrospinning[29]. However, NIPS is the most preferred method for industrial production of porous membranes [30]. The NIPS process generates porous membranes that are composed of membrane-forming polymers and additives, which are required to be insoluble in non-solvents. In contrast, both solvents and non-solvents are miscible [31].

Although PVDF membranes are highly effective in water treatment, they are prone to fouling during the filtration process [32]. Hydrophobic membranes are especially vulnerable to fouling when used to treat aqueous solutions containing organic matter [33]. These substances can easily adhere to the membranes, clogging pores, reducing efficiency, and increasing cost [34]. Research has shown that membrane fouling is more resistant to hydrophilicity increases [35]. Hence, several methods have been developed to enhance the hydrophilicity of PVDF membranes. Hydrophilic materials are typically incorporated through surface coatings or in situ blending methods. Several studies have reported that PVDF was blended with hydrophilic materials to improve the hydrophilicity of the membrane. A blended material can comprise hydrophilic polymers such as PMMAs (poly (N-isopropylacrylamide) [36], PVP (polyvinylpyrrolidone) [37], CAs (cellulose acetates) [38], and nanofillers such as ZnO [39], titanium dioxide [40], silver particles [41], or cyclodextrin [42]. By incorporating nanocomposites during phase inversion, membranes can be significantly improved in terms of their hydrophilicity and antifouling properties by altering their morphology [43]. This has been demonstrated by a number of studies, including one by Roshani et al. [44] that found an improvement in both wettability and salt rejection rate of PVDF membranes following the addition of PS/ZnO nanocomposites. Furthermore, Ma et al.[45] observed that reducing the size of TiO_2 nanoparticles in PVDF membranes enhances their antifouling properties, while Peyravi et al. [46] found that adding different amounts of ZnO nanoparticles to PVDF membranes can directly affect the membrane contact angle, resulting in increased hydrophilicity.

β-cyclodextrin (β-CD) is a molecule consisting of seven glycosyl units and is considered the most preferred type of cyclodextrin in terms of both performance and cost [47]. Each cyclodextrin is a torus-shaped molecule that resembles a doughnut [48], with a hydrophobic cavity inside and a hydrophilic surface outside [49]. The hydroxyl groups present in β-CD are crucial in its use in several applications, and their substitution with other functional groups can improve its performance and functionality [50]. The ability of β-CD to enhance the adsorption performance of several common adsorbents has been extensively studied. For example, Mohammadi et al. [51] studied the performance of a composite adsorbent, (MWCNTs/Gly/ β-CD), for removing various dyes from aqueous solutions. Incorporating β-CD into MWCNTs improved the adsorption capability significantly due to β-CD's inner hydrophobic cavity and outer multiple hydroxyl groups, which can form complexes with organic dyes and pollutants. Recent studies have focused on incorporating β-CD and its derivatives into complex membrane systems [52]. For instance, Yuancai et al. [53] developed a cellulose nanofiber membrane loaded with porous β-CD to treat bisphenol pollutants. The study found that the volume of treated water in the CA/P.β-CD membrane was 14.5 times greater than that in the control

 doi:10.20944/preprints202404.1247.v1

membrane sample. Nanomaterials can also be functionalized with β-CD, resulting in a hybrid material with synergetic properties. Liu et al. [54] reported the modification of graphene oxide (GO) with β-CD through chemical grafting to enhance the permeability of the membrane. β-CD improves water flux by expanding GO's interlayer without affecting rejection efficiency. However, only a small amount of research has been conducted on the direct blending of PVDF membranes with β-CD.

This research article focuses on preparing β-CD modified PVDF membranes to effectively remove dye molecules from textile wastewater. β-CD molecules can enhance the hydrophilic and dielectric properties of membranes. Through various characterization methods, we confirmed that the addition of β-CD significantly improves the morphology, hydrophilicity, dielectric properties, and performance of the modified PVDF membranes. The addition of β-CD results in a dielectric exclusion of dyes, which has not been well demonstrated elsewhere, proving our confidence. Our research indicates that we are leading the way in developing innovative solutions to guarantee access to clean water.

2. Materials and Methods

2.1. Materials

Poly(vinylidene fluoride) (PVDF, average Mw ~534,000), Polyvinylpyrrolidone (PVP, Mw ~ 40k) Methylene blue (MB, ≥95%), Methyl red (MR, BioReagent, ≥95%), and Rose bengal (RP, ≥95%,) were purchased from Sigma-Aldrich, St. Louis, MO, USA. Brilliant blue (BB, Reagent European Pharmacopoeia) was bought from Fisher Scientific GmbH, Schwerte, Germany. Dimethylformamide (DMF, 99.9%) was acquired from Sigma-Aldrich, USA. Deionized water (18 MΩ) was produced using the ELGA Deionization System.

2.2. Membrane Preparation

The PVDF membranes were prepared using the phase inversion method. PVP and β-CD were dissolved in DMF at a fixed ratio of 1 wt%. At a constant speed, 3.33g of PVDF powder was dissolved in 20g of DMF and heated to 50°C. After dissolving polyvinylidene fluoride (PVDF) 0.223 g of additives consisting of polyvinylpyrrolidone (PVP) and β-cyclodextrin (β-CD) were added to the solution. The ratio of PVP to β-CD was varied between 1-x% and x%, where $0 \leq x \leq 1$. The mixture was stirred for 4 hours to ensure complete homogeneity. The solution was then degassed overnight to remove any bubbles that may have formed during stirring. Using a Porometer MEMCAT machine, the dope solution was cast onto a clean stainless-steel plate with a gap size of 250μm at a temperature of 40 degrees. The casted membrane was then immersed in deionized water for 24 hours. After removal, the membrane was dried, cut to size, and stored for future use. The membranes were named M_0, M_1, M_2, M_3 and M_4 for respectively PVDF-PVP, PVDF-$PVP_{0.75}$ β-$CD_{0.25}$, PVDF-$PVP_{0.5}$ β-$CD_{0.5}$, PVDF-$PVP_{0.25}$ β-$CD_{0.75}$ and PVDF-β-$CD_{1.0}$.

A membrane named M_5 was created using identical conditions to those used in the production of membrane M_1. However, instead of b-CD molecules, a-CD molecules were used in the preparation of M_5.

2.3. Pure Water Flux and Wettability

A flat sheet membrane separation unit was used to separate a sample. The membrane was cut and shaped to fit the fouling unit cell. Before use, the sample was wetted with isopropanol and distilled water was fed into the unit. The permeate flux of pure water was measured at a working pressure of 80 KPa. (Equation (1)):

$$J_{W.1} = \frac{V}{A \times t} \quad \textbf{(Eq.1)}$$

Where $J_{W.1}$ (L m^{-2} h^{-1}) is the water flux, t (h) is flowing time, V (L) is solution volume, and A(m^2) is membrane effective area.

Determining the wettability of membranes is an important process, which can be achieved through contact angle measurements. In this study, we used the Attension Theta Flex instrument

 doi:10.20944/preprints202404.1247.v1

from Bioline Scientific to measure the pure water contact angle (CA) of the membranes, using the sessile drop method at room temperature. To ensure accurate results, all fabricated membranes were fully dried, cut into 20 mm × 1.5 mm strips, and attached to the sample holder. A 3 μL pure water droplet was then carefully dropped onto a clean and well-dried membrane surface using a micro-syringe. We performed a Triblet test for each sample at different locations, and the results were averaged to obtain an accurate contact angle. This method provides important insights into the properties of the membranes, which can help us to optimize their performance.

2.4. Separation Performances of Membranes and Antifouling Test

This study aimed to examine and optimize the separation capability of modified PVDF membranes on four different dyes: Neutral (Methyl Red, MR), cationic (Methylene Blue, MB), and two anionic (Brilliant Blue(BB), Rose Bengal(RB)). In the first stage, we tested the membranes' ability to separate (MB) solution. During the second stage, we evaluated the performance of the optimized membrane by supplying three-component dye solutions to the filtration system. Each experiment used a new membrane sample, which was fixed to the membrane cell. The results from this study will help to enhance the development of improved membrane technologies for dye separation.

The rejection ratio of each dye solution (at a concentration of 10 mg L−1) was determined by testing under a working pressure of 80 KPa. The maximum absorbance measurements were taken using a Shimadzu UV-160 spectrophotometer. The concentrations were used to calculate the percentage of solute rejection, which is expressed by Equation (2).

$$\mathbf{R\ \%} = \frac{C_f - C_p}{C_f} \boldsymbol{X}\ \mathbf{100} \qquad \textbf{(Eq.2)}$$

Where R is the solute rejection (%), C_P and C_f are the permeate and feed concentration (mg L^{-1}), respectively.

The performance of membrane antifouling was analyzed using a three-cycle flotation process. First, the pure water flux ($J_{w.1}$) was measured at a fixed volume for a certain time. After that, the flux of dye solution through the membrane was measured as (J_P). Then, the fouled membrane was cleaned with deionized water, and the water flux ($J_{w.2}$) was recorded again. Next, the flux attenuation curves of the membrane sample were plotted, and the flux recovery ratio (FRR) was calculated using (Equation (3)).

$$\mathbf{RFR\ (\%)} = \mathbf{(1-}\ \frac{J_P}{J_{W.1}}\mathbf{)} \times \mathbf{100} \qquad \textbf{(Eq. 3)}$$

To calculate the system resistance due to various fouling mechanisms, Darcy's law was applied:

$$\boldsymbol{J} = \frac{\triangle \boldsymbol{P}}{\mu(\boldsymbol{R_m} + \boldsymbol{R_c} + \boldsymbol{R_f})} \qquad \textbf{(Eq. 4)}$$

J is the permeate water flux ($m^3\ m^{-2}\ s^{-1}$), ΔP is the applied pressure (kPa), μ is the water viscosity (Pa.s), R_m represents the hydraulic resistance (m^{-1}), R_f is a measure of fouling resistance (m^{-1}) and R_c is a concentration polarization resistance (m^{-1}).

The total resistance (R_T) was determined using the resistance-in-series model by combining all filtration resistances. The following equation (Equation (5)) was used to calculate R_T:

$$\mathbf{R_T = R_M + R_F + R_C} \qquad \textbf{(Eq. 5)}$$

R_M is caused by porous sizes and distributions, membrane thickness, as well as the hydrophilic and hydrophobic properties of the membrane. It can be measured using (Eq. 6):

$$\boldsymbol{R_m} = \frac{\triangle \boldsymbol{P}}{\mu\,(\boldsymbol{J_{w.1}})} \qquad \textbf{(Eq. 6)}$$

R_F represents the resistance resulting from pore adsorption, pore blocking, and cake deposition. It was calculated based on the measurements of water flux following the pollutant rejection experiment ($J_{w.2}$) as described in (Equation (7)):

$$\boldsymbol{R_f} = \frac{\triangle \boldsymbol{P}}{\mu\,(\boldsymbol{J_{w.2}})} - \boldsymbol{R_m} \qquad \textbf{(Eq. 7)}$$

Finally, subtracting all other resistances from R_T (Equation (8)) gives the final value of R_C.

$$\boldsymbol{R_c} = \boldsymbol{R_T} - \boldsymbol{R_m} - \boldsymbol{R_f} \qquad \textbf{(Eq. 8)}$$

 doi:10.20944/preprints202404.1247.v1

2.5. Porosity

The porosity of a membrane is a well-defined characteristic that determines the amount of void space present within its volume. With applying the gravimetric method, represented by Equation (9), we can confidently measure this property, providing a solid foundation for further exploration and innovation.

$$\varepsilon = \frac{W_2 - W_1}{\rho_w \times A \times h} \quad \textbf{(Eq .9)}$$

The wet and dry weights of membranes are w_1 and w_2, respectively. The density of water (ϱ_w) is 0.998 g cm^{-3} and A is the membrane area (cm^2).

The Elford-Ferry equation (Equation (10)) is a widely used method for estimating the average pore size of membranes. This equation considers the membrane thickness, porosity, and hydraulic permeability to determine the average pore size. By accurately estimating the average pore size, we can better understand the transport properties of the membrane, which is crucial for many applications such as water purification, gas separation, and biomedical devices. Additionally, the Elford-Ferry equation is versatile and can be applied to various membranes, from microfiltration to ultrafiltration. Therefore, it is an essential tool for researchers and engineers in membrane technology.

$$rm = \sqrt{\frac{(2.9 - 1.75\,\varepsilon) x 8\eta\, d\, Q}{\varepsilon\, x\, A\, x\, P}} \quad \textbf{(Eq. 10)}$$

Where η is the viscosity of water (8.9×10^{-4} Pa.S). Q is filtration volume ($m^3\ s^{-1}$), A is the membrane area (m^2), P represents the operating pressure (MPa) and d (m) is the membrane thickness, measured by a digital micrometer.

2.6. Characterization

The membrane's structural characteristics were identified through several methods, including an X-ray diffraction (XRD) analysis, attenuated total reflectance infrared spectroscopy (ATR-IR), and atomic force microscopy (AFM). XRD data was obtained using a Ni-filtered Cu Kα radiation source (λ = 1.54184 Å) and an automatic diffractometer (Philips Panalytical X'Pert ProMPD), while ATR-IR was used to determine the chemical composition of the modified membrane surfaces using a Bruker TENSOR27 FT-IR spectroscopy. The membrane's thermal stability was evaluated through a thermogravimetric analysis (TGA) using Shimadzu TGA-50 in a nitrogen-containing atmosphere. SEM and AFM were used to examine the membrane's surface morphology and topography, respectively. Prior to scanning, the membrane samples were dipped in liquid nitrogen for cutting to preserve cross-sectional structure. The average plane roughness (Ra) and root mean square roughness (Rms) were also measured to evaluate surface roughness. These methods provided a comprehensive understanding of the membrane's characteristics and improved its performance.

3. Results and Discussion

The X-ray diffraction patterns of neat PVDF and β-CD modified membranes are shown in Figure 1. The pure PVDF membrane diffraction pattern displays two strong peaks at 18.4° and 20.3°, and two weaker peaks at 36.3° and 41.1°. These peaks indicate the presence of nonpolar α and polar β crystalline phases [55,56]. In particular, the α phase peaks can be observed at 2θ = 18.4° [57] and 40.5° [58]. The β phase shows a strong diffraction peak at 2θ = 20.3°, which is attributed to the sum of the diffraction in the (110) and (200) planes, plus a smaller peak at 2θ = 36.4° [59].

 doi:10.20944/preprints202404.1247.v1

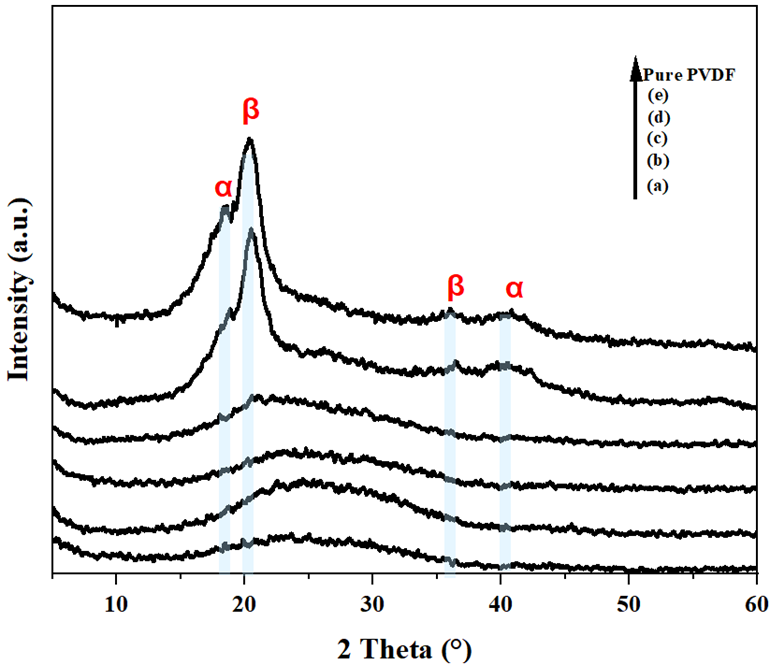

Figure 1. XRD diffraction patterns of (**a**) M_1, (**b**) M_2, (**c**) M_3, (**d**) M_4, and (**e**) M_0 pure PVDF.

Figure 1 shows that the presence of PVP, an amorphous polymer, has affected the diffraction patterns of the modified membranes. According to Xiang et al. [60], PVDF's miscibility with PVP affects its XRD diffraction peaks, gradually shifting from crystallized PVDF to amorphous PVP. Eren et al. [61] explain that forming hydrogen bonds between PVDF hydrogen atoms and PVP carbonyl groups may destabilize the crystalline segments, reducing the crystallinity. However, the membrane with 1% β-CD (Figure 1(M_4)) follows the same diffraction pattern as pure PVDF, exhibiting all four peaks without any noticeable shift in their position. X-ray diffraction confirmed the presence of residual PVP in PVDF membranes, while β-CD presence shows no effect on the polymer crystallinity.

To determine the chemical composition of M_i membranes attenuated total reflectance infrared spectroscopy (ATR-IR) is investigated, and the results are presented in Figure 2. The analysis revealed that the PVDF membrane spectrum displayed peaks at 1405 cm^{-1} and 1168 cm^{-1}, which were attributed to the stretching vibrations of CH_2 and CF_2 [62]. Additionally, the peaks at 878 cm^{-1} and 840 cm^{-1} were caused by the stretching vibrations of C–C and C–F bonds [63]. The peak at 2900 cm^{-1} reflected $–CH_3$ band vibration and stretching [64]. The peak at 1660 cm^{-1} may be attributed to C=O groups from PVP and/or β-CD water deformation bands of H–O–H for modified membranes. [65,66]. Moreover, we found an absorption band in the range of 3200-3600 cm^{-1}, which was attributed to O–H stretching [67]. This peak was caused by the presence of PVP and β-CD. The O–H peak in modified membranes indicated that β-CD was successfully incorporated into the polymer matrix. Overall, these findings provide valuable insights into the chemical composition of the fabricated membranes, which can be useful in further optimizing their performance.

 doi:10.20944/preprints202404.1247.v1

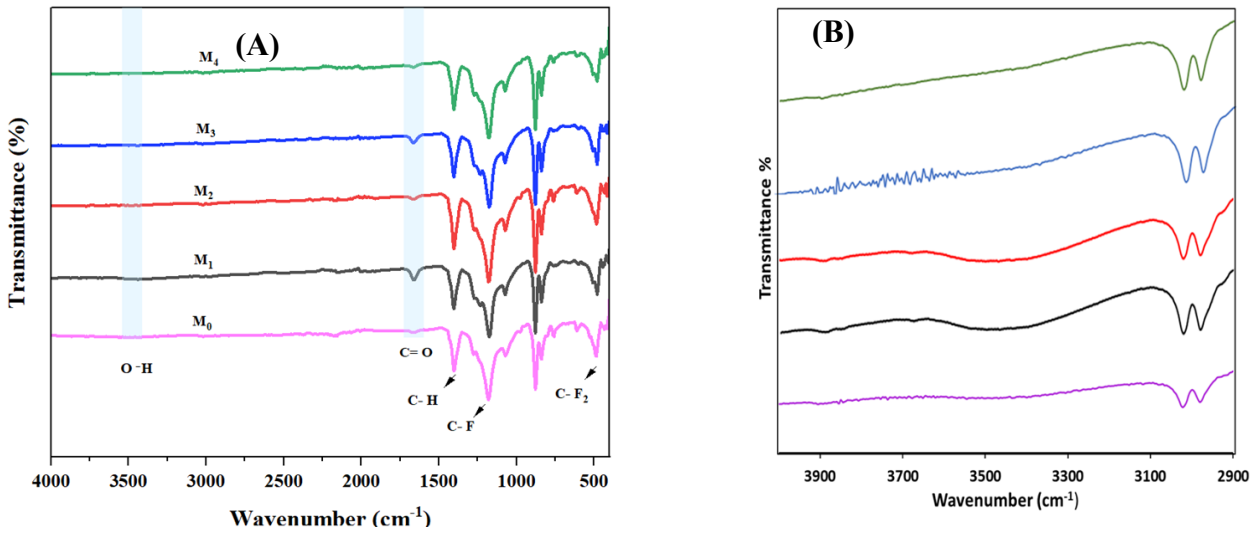

Figure 2. (**A**) ATR-IR spectra of PVDF-PVP$_{(1-x)}$- β- CD$_{(x)}$ membranes: M$_0$ (x=0), M$_1$ (x=0.25), M$_2$ (x=0.50), M$_3$ (x=0.75) and M$_4$ (x=1.0). (**B**) Zoom 2900-4000 cm^{-1}.

Figure 3 presents the Raman spectra of β -CD modified PVDF. The Raman shift observed at 1100 cm^{-1} corresponds to symmetric in-plane C–C stretching motion [68,69]. There is no question that the intensity of the compound is entirely dependent on the precise loading of beta-cyclodextrin (βCD) present in the mixture. The increased intensity of the guest molecule beta-cyclodextrin (βCD) from M$_1$ to M$_4$ membranes provides important insight into the membrane structure. By comparing the relative intensities of the peak at 1100 cm^{-1}, we could subtract the free βCD membrane (M0) spectrum from the complex ones (Figure 3B). Interestingly, in the case of M$_3$ (0.75 w% βCD), the relative intensity was almost the sum of M$_1$ and M$_2$, and the sum of M$_1$ and M$_3$ for M$_4$. These findings can help us to ascertain a homogeneous distribution of βCD in the membrane.

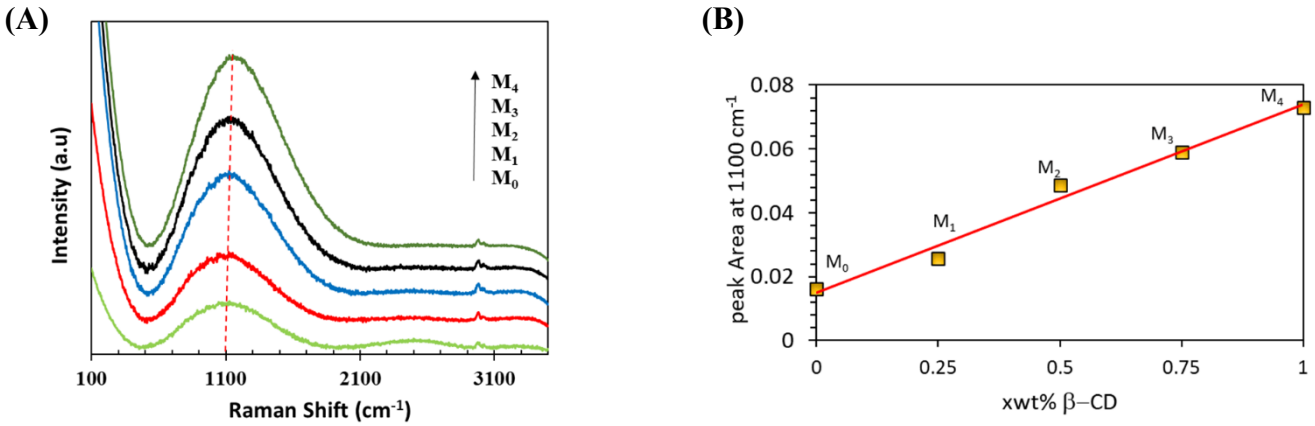

Figure 3. (**A**) Raman spectra of PVDF-PVP$_{(1-x)}$- β- CD$_{(x)}$ membranes: M$_0$ (x=0), M$_1$ (x=0.25), M$_2$ (x=0.50), M$_3$ (x=0.75) and M$_4$ (x=1.0). (**B**) peak area at 1100 cm^{-1} versus b-CD loading.

To better understand how the presence of β-CD affects the membrane structure and pore morphology, we conducted scanning electron microscopy (SEM). Figure 4 provides valuable insights into the cross-sectional and surface morphology of the blended membranes. We have analyzed SEM images of the membrane surface and found the emergence of pores of different diameters, depending on the b-CD loading (Figure 4). Further statistical analysis on 200 pores revealed that the highest mean pore average of 710 nm was observed for M$_0$ (1 wt% PVP). M$_1$ exhibited an optimal performance with a bCD loading of 0.25 wt%, which resulted in a pore diameter range of 345 nm. Subsequently,

 doi:10.20944/preprints202404.1247.v1

with increased bCD loading, a decrease in pore diameter was observed, with 1 wt% of bCD resulting in a diameter of 205 nm (Table 1). This information could be vital in understanding the behavior of the membrane and improving its performance. In particular, the cross-sectional view of M_0 membrane shows the presence of large finger-like macro-voids and cavities with a porous surface layer (fig.4 M_0), a common feature of PVDF/PVP membranes fabricated using NIPS [70]. Figure 3 (M_1, M_2, M_3, M_4) demonstrates how incorporating β-CD nanofillers into the membrane can alter the pore morphology. At low β-CD loadings (0.25-0.5 wt%), there is an improvement in the formation of finger-like pores and an increase in their diameter. According to Zheng et al. [71], the kinetics of phase inversion significantly impact membrane formation. Solid and liquid polymer phases are formed when a cast dope solution is dipped into a non-solvent [72].

NIPS is a necessary process that involves either instantaneous or delayed de-mixing, leading to the formation of different types of pores [73]. Ho-Taek states that hydrophilic additives work as de-mixing enhancers for NIPS [74]. Thus, hydrophilic additives affect phase-inversion kinetics, suggesting that β-CD may be directly related to (OH) groups, which increase mass transfer across membranes [75]. During the instantaneous de-mixing process, nonsolvent diffuses more quickly from the cast membrane, resulting in greater pore channels and a faster solidification rate. However, it's important to note that the impact of β-CD's hydrophilicity on the process is limited by the presence of PVP contents in the membrane. As such, it's important to maintain the right balance of PVP content to ensure that the pores have the right size and density. By carefully monitoring the process and measuring the porosity, mean pore size, and thickness of modified membranes, we can improve the quality and effectiveness of the NIPS process (Table 1).

The data in Table 1 suggests that the thickness of the membrane varies depending on the amount of βCD and PVP present simultaneously. Interestingly, for low ⌾CD loading (0.25 wt%), the membrane thickness remains unchanged compared to the M_0 membrane. However, as the ⌾CD loading increases, the membrane thickness decreases in the following order : M_2 (100 μm) > M_3 (89 μm) > M_4 (80 μm). These findings are consistent with a similar study investigated by Morihama et al. [74], where adding Nano clay to PVDF membranes with and without PVP produced different results. Specifically, adding only clay nanoparticles resulted in a thin membrane (33.1 μm) with a sponge-like structure, while the PVDF-PVP (1 wt.%) Nanoclay (2wt.%) membrane resulted in a thicker membrane (83 μm) with a finger-like structure. Furthermore, the porosity of the membrane is highly affected by PVP loading. The M_0 membrane has a porosity of 47% against 16% for a PVP-free membrane, indicating the importance of PVP in achieving high porosity. Interestingly, an optimum porosity of 71% is observed for M_2, which contains 0.75 wt% PVP with 0.25 wt% ⌾CD. The Elford-Ferry equation yields a higher pore size diameter than SEM analysis, particularly for M_2 and M_3. This discrepancy can be explained by the fact that SEM analysis only considers the surface while the Elford-Ferry equation considers both surface pores and internal voids.

Table 1. Membrane properties: thickness, porosity, average pore diameter from SEM, average pore size from Elford-Ferry equation, mean roughness (Ra), the root mean square of the Z data (Rq), and the mean difference between the highest peaks and lowest valleys of the membranes (Rpv).

Membrane	b-CD (wt.%)	PVP (wt.%)	Thickness (mm)	Porosity (%)	Contact angle (°)	Average pore diameter (nm)		Atomic Force Microscopy (AFM)		
						SEM*	Elford-Ferry equation	R_a (nm)	R_q (nm)	R_{pv} (nm)
M_0	0	1.00	110 ±1	47	72.6±1.8	710	500	81-101	99-118	417-437
M_1	0.25	0.75	110 ±1	72	54.6±1.8	345	913	29-26	31-33	115-124
M_2	0.50	0.50	100 ±1	38	63.7±0.8	508	835	50-59	66-68	281-334
M_3	0.75	0.25	89 ±1	31	80.9±1.1	525	176	47-52	57-63	217-28
M4	1.00	0	80 ±1	16	87.1±1.5	205	-	58	71-72	304-310

*Average pore diameter calculated from surface scanning of 200 pores.

 doi:10.20944/preprints202404.1247.v1

The roughness of a membrane is a crucial factor that significantly impacts fouling performance and surface contact angle. It is well-established that molecules tend to accumulate more readily on rough membrane surfaces, leading to increased fouling. [76]. In contrast, smooth surfaces are less likely to accumulate fouling in the long term. To investigate the effect of β-CD loading on membrane surface roughness, a three-dimensional AFM was performed on an 8 μm x 8 μm area. The results are displayed in Figure 5.

The roughness parameters of PVDF-PVP-β-CD are summarized in Table 1. These parameters are expressed in terms of the mean roughness (Ra), the root mean square of the Z data (Rq), and the mean difference between the highest peaks and lowest valleys of the membranes (Rpv). The surface of M0 membrane (Fig. 5, M0) clearly displays several large peaks resulting from its highly rough texture (Ra ~81 nm). This can be confidently attributed to the presence of PVP as a pore agent, which has a large molecular size [77]. Upon reducing PVP contents, the surface appears smoother with smaller peaks and decreased roughness. The presence of β-CD molecules decreased the Ra values, reaching an optimal value of 29 nm at 0.25 wt% β-CD. It's worth noting that the Rq values exhibited a similar trend to that of the roughness. This information could provide valuable insights for further analysis and improvements. Blended β-CDs membranes showed lower roughness compared to PVDF-PVP(1). The lowest roughness was assigned to M1 (0.25 wt% βCD) and a slight increase was recorded with further loading due to the aggregation phenomena of nanomaterial [78]. The above statement confirms the previous observations on how hydrophilic additives affect the roughness of hydrophobic membranes. In a study conducted by Mabusha et al. [79], it was found that incorporating 1% f-CNT resulted in a three-fold decrease in roughness for PSF/PES membranes. This decrease was attributed to the impact of hydrophilic additives on the phase inversion kinetics.

 doi:10.20944/preprints202404.1247.v1

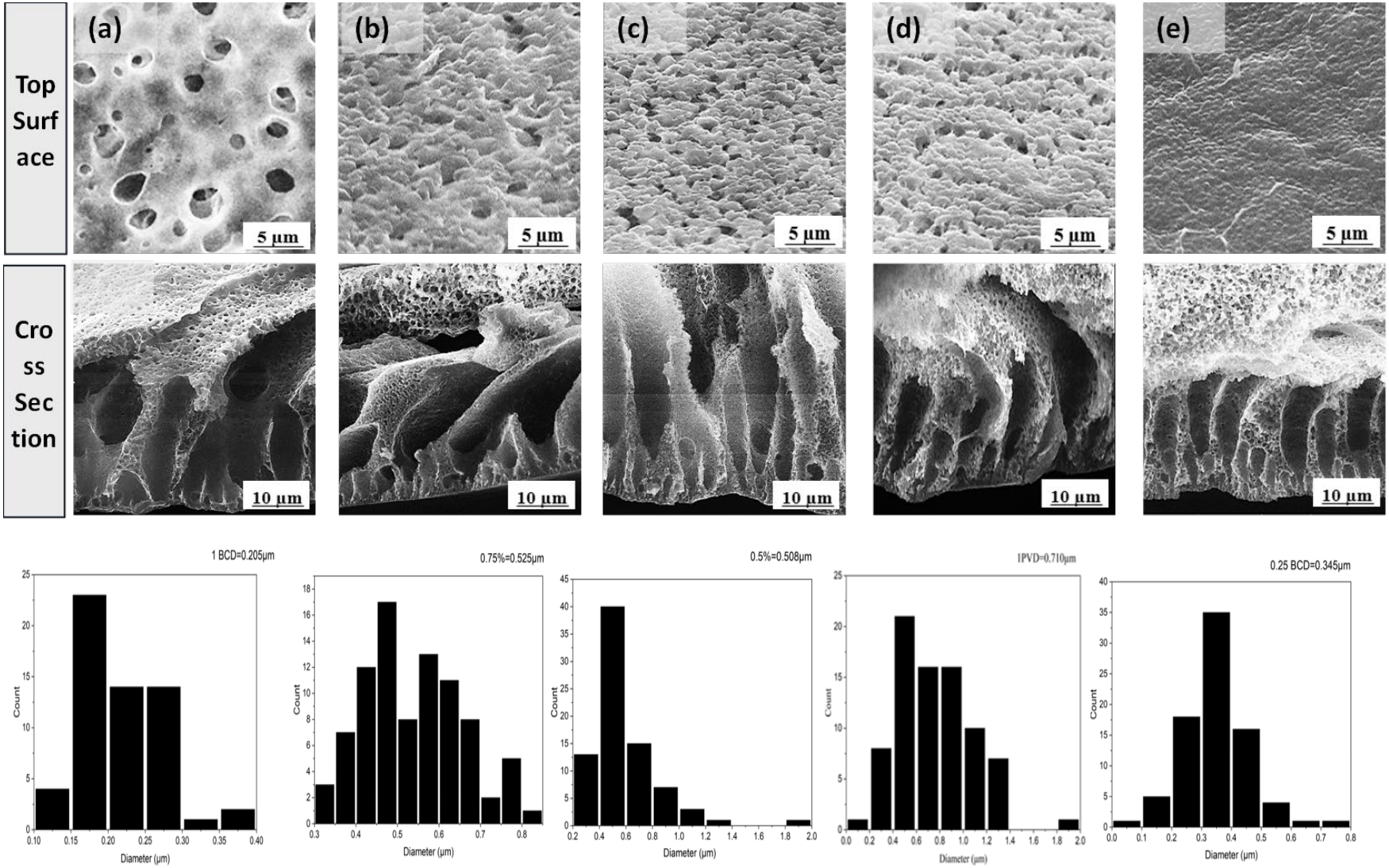

Figure 4. SEM images (surface and cross section) and average pore diameter of PVDF-PVP$_{(1-x)}$- β- CD$_{(x)}$ membranes: (**a**) M$_0$ (x=0), (**b**) M$_1$ (x=0.25), (**c**) M$_2$ (x=0.50), (**d**) M$_3$ (x=0.75) and (**e**) M$_4$ (x=1.0).

 doi:10.20944/preprints202404.1247.v1

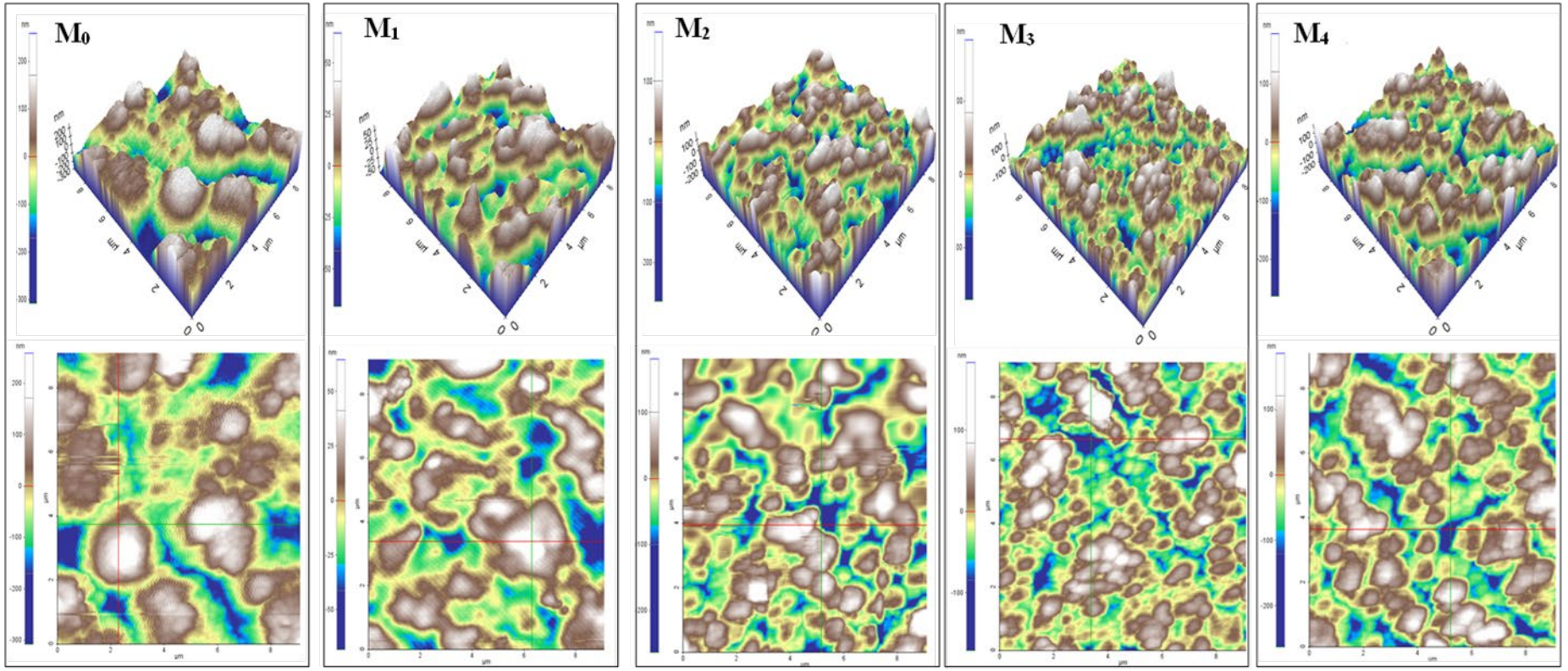

Figure 5. AFM images of PVDF-PVP$_{(1-x)}$- β- CD$_{(x)}$ membranes: **M$_0$** (x=0), **M$_1$** (x=0.25), **M$_2$** (x=0.50), **M$_3$** (x=0.75) and **M$_4$** (x=1.0).

Preprints.org (www.preprints.org) | NOT PEER-REVIEWED | Posted: 18 April 2024 doi:10.20944/preprints202404.1247.v1

The thermal stability of M_0 to M_4 membranes was evaluated using TGA. Figure 6 data indicates that all the membranes maintain stability up to 370°C. This temperature seems to allow for very little molecular water to evaporate. Between 370°C and 480°C, PVP membranes (M_0 to M_3) decompose in two stages. In contrast, the PVP-free membrane (M_4) degrades in a single step between 440°C and 490°C. Studies conducted earlier [80] showed that PVP decomposition is responsible for weight loss at approximately 370°C. The actual weight loss observed during the experiments is consistent with the theoretical calculations of PVP content in each membrane. The observed weight loss percentages at 370°C are 8%, 5%, 3%, 1.5%, and 0% for M0, M1, M2, M3, and M4. In Figure 6B, it is shown that the temperature at which the maximum weight decomposition took place was 460°C for M_0 (1wt% PVP). Upon the addition of β-CD, it was noted that the temperature increased to 471°C. This change indicates that the second-stage decomposition occurred at a higher temperature, enhancing the modified membranes' stability. The improved thermal stability of the modified membranes can be attributed to alterations in surface roughness, as observed in AFM measurements. In a study conducted by Mohammed et al. [81], it was shown that the grafting of poly-HEA onto PVDF resulted in a reduction in surface roughness and contact angle, which was associated with an enhancement in thermal stability.

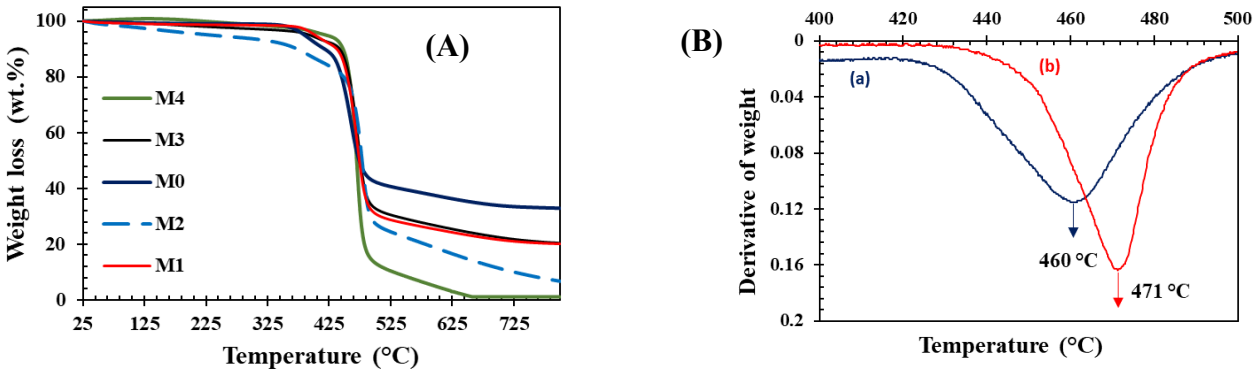

Figure 6. (**A**) TGA of M_0, M_1, M_2, M_3 and M_4 membranes and (**B**) derivatives weight loss of a) M_0 b) M_1 membranes.

The contact angle (CA) and permeate flux are key indicators of a membrane's wettability and hydrophilicity. We measured water contact angle measurements to measure the modified membrane's hydrophilicity (Figure 7).

Figure 7 shows that M0 membrane, has a water contact angle of 72°, is highly hydrophobic. On the other hand, upon the addition of 0.25wt% β-CD, the CA decreases by 23%, indicating better hydrophilicity. According to Zongxue et al. [82], the presence of hydroxyl groups on the outer surface of the blended β-CD molecules enhanced the water-membrane interactions in the PVDF membrane. Herein, the incorporation of β-CD in the blended membrane significantly enhances the pure water flux from 48 to 241 LMH for M2 (0.25 wt%β-CD). By contrast, the water flux decreases dramatically for higher bCD loadings. This result can be supported by the existence of a synergetic effect between PVP (pore former) and bCD (polarity tuning). Herein, incorporating β-CD onto the membrane increased its permeability due to the higher porosity created by an enlargement in pore size, as seen in SEM images. The hydrophilicity also increased, allowing instant wetting of the membrane surface and faster water flow through better transfer channels. However, when the content of β-CD exceeded 0.5%, the water flux sharply decreased, possibly due to a change in morphology. The adjusted PVDF membrane's average pore size increases simultaneously with β-CD until it reaches a breaking point. Beyond 0.5% loading, the membrane pores volume decreased, making it difficult for water to transport across the membrane due to the high reduction of PVP. Overall, M4 membrane had the highest surface contact angle (87°), which prevented water from passing through under 80Kpa working conditions.

An investigation was conducted to assess the enhancement in membrane flux by measuring the membrane resistance (Rm) (supplementary information Figure S1). The internal resistance of the M0

 doi:10.20944/preprints202404.1247.v1

membrane (1wt% PVP) is found to be ~470 m^{-1}, while the β-CD modified membranes exhibit a significant decrease in resistance at low loading. The reduction in resistance caused by the introduction of β-CD in membranes could be due to the improvements in hydrophilicity, pore size, and roughness. The increase in pore size of the membrane reduces the mass-transport resistance and escalates the permeated flux, leading to better membrane wetting. Among the modified membranes, M1 (0.25wt% β-CD) shows the lowest resistance (93 m^{-1}), consistent with the water flux values.

Table 2 summarizes the effects of various additives on water flux and contact angle on PVDF. Various blending methods were used, including nanomaterial, nanomaterial-polymer, and polymer. The weight percentages of PVP (nanofiller) and PVDF were varied between 1-3% and 15-18%, respectively. At the same PVP loading (1wt%), the addition of nanomaterial enhances the water flux and lower the contact angle. For example, with the addition of 0.4 wt% Ag/ZrO_2, the contact angle decreases from 82.7° to 60° and yields better water flux [83]. Incorporating Cu_2S (1 wt%) into the membrane has a beneficial impact on its polarity, resulting in a reduction in contact angle and a significant increase in water flux, improving the overall efficiency of the membrane [84]. For higher PVP loading (3wt%), the addition of GO-Ag composite (0.15wt%) results in polarity and flux enhancement [85]. With the incorporation of just 0.36 wt.% of β-CD-HNTs, the water flux experiences a slight yet remarkable boost [86]. These comparisons provide further insight for conducting deeper experiments. However, the varying parameters and loading used in the literature make comparisons difficult. Other research groups have explored using nanomaterials and/or polymers as additives in PVDF membranes without using PVP. Various additives were investigated to enhance the properties of the PVDF membrane. Among these were 10 wt% of PEG200 and 0.1 wt% of LDH [87], PAN-TNT (1-3 wt%) [88], and Styrene acrylonitrile (SAN) [89]. These additives result in a more hydrophilic membrane; there is no doubt that water flux enhancement has occurred. Our work has conclusively demonstrated that adding a merely 0.75 wt% PVP and 0.25 wt% bCD results in a significantly improved hydrophilic PVDF membrane, with a remarkable enhancement of 345% in water flux.

Table 2. Water flux and contact angle for modified PVDF membranes.

PVDF (wt.%)	PVP (wt.%)	Additives	Blending Method	Contact Angle (°)	Water Flux ($L.m^{-2}.h^{-1}$)	References
15	1	Ag/ZrO_2 (0-0.4 wt.%)	nanomaterial	82.7° to 60°	40 to 137	[83]
18	1	Cu_2S (0-1 wt.%)	nanomaterial	77.8° to 66°	152 to 248	[84]
17	3	GO-Ag composite 0-0.15 wt.%)	nanomaterial	82° to 63°	110 to 177	[85]
18	3	β-CD-HNTs (0-0.36 wt.%)	nanomaterial	84° to 57°	23 to 69.5	[86]
15	-	PEG200[a] (10 wt.%) LDH[b] (0-0.1 wt.%)	nanomaterial /polymer	89° to 62°	164 to 213	[87]
15	-	PANI -TNT[c] (x=1-3 wt.%)	nanomaterial /polymer	102° to 66°	312 to 484	[88]
17.5	-	SAN[d] (x=0,10, 20, 60, 100 wt.%)	polymer	82°to 63°	24 to 245	[89]
15	0.75	β-CD (0.25 wt.%)	organic molecule	72° to 55°	48 to 214	This work

[a] PEG200, Poly(ethylene glycol); [b]Layered double hydroxides, LDH (Mg-Al); [c]PANI (polyaniline), TNT(titanium nanotube) ; [d]Styrene acrylonitrile (SAN).

 doi:10.20944/preprints202404.1247.v1

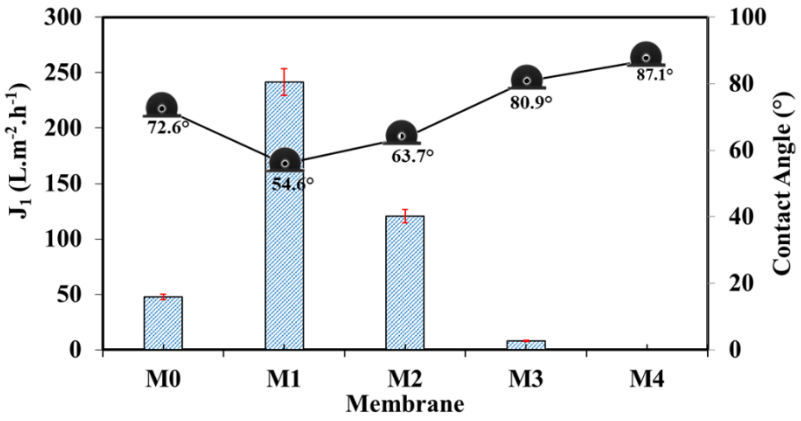

Figure 7. Pure water flux of PVDF-PVP$_{(1-x)}$- β- CD$_{(x)}$ membranes: M_0 (x=0), M_1 (x=0.25), M_2 (x=0.50), M_3 (x=0.75) and M_4 (x=1.0) and their corresponding contact angle values.

The selectivity (or separation power) of the membrane is not governed only by size effects (linked to the relative sizes of pores and solutes) but also by interactions of electrostatic origin, including Coulomb forces (due to the surface charge of the membrane) and very probably exclusion dielectric phenomena (due to differences in dielectric constant between the solution in the nanopores, the membrane material and the external solution). To achieve the desired results, it is crucial to thoroughly analyze the structural characteristics of the membranes, including pore radius, thickness, and porosity, in addition to examining their electrical and dielectric properties.

In Figure 8, the behavior of the dielectric constant (ε') of a PVDF membrane is shown for different β-CD substitution ratios. The measurement was taken in the frequency range 10 – 10^6 Hz and with zero Vdc. It is observed that the dielectric constant (ε') is not constant and varies with frequency. The value of ε' at low frequencies is higher than at high frequencies. The β-CD substitution ratio, represented by the variable 'x', affects the dielectric coefficient. The dielectric coefficient also increases as the β-CD substitution ratio increases (x=0, 0.25, 0.5, 0.75, 1). For example, for the x=1 value, the value of ε' is approximately 34.4, corresponding to a 40% increase in the dielectric constant. This is a significant result. The high value of ε' (≈ 34.4) at low frequencies is due to the influence of Maxwell-Wagner-Sillars (MWS) interface polarization [90]. The results presented in Figure 8B demonstrate a clear correlation between the conductivity value and frequency, particularly for increasing ratios of β-CD substitution. Notably, beyond 10^5 Hz, the ac conductivity values for M_0 (0 wt% β-CD) and M_4 (1.0 wt% β-CD) reached 1.36x10^{-4} and 2x10^{-4} S/cm values at 1x10^{-7} Hz, respectively. These findings suggest that β-CD substitution may play a key role in enhancing the conductivity of the material under investigation. This result may contribute to dye separation as the membrane and solution dielectric constant differ.

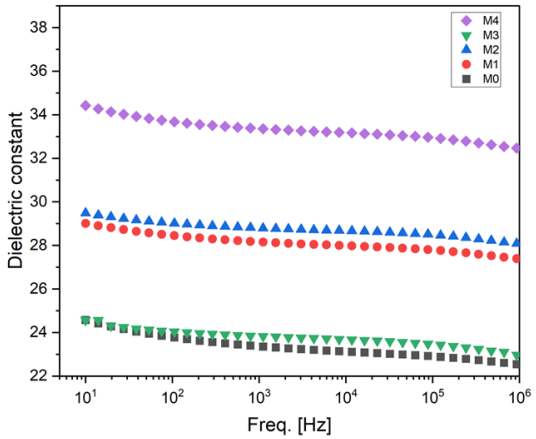

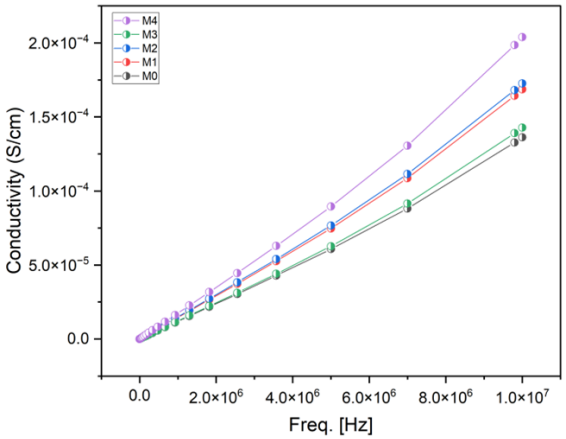

 doi:10.20944/preprints202404.1247.v1

Figure 8. (**A**) Dielectric constant behavior as a function of frequency and (**B**) Ac conductivity behavior for of M_0, M_1, M_2, M_3 and M_4 membranes.

To test the effectiveness of a membrane's antifouling properties, a multicycle filtration method was used. The first cycle involved allowing pure water to pass through the membrane for a period of time. In the second cycle, a solution containing MB (10 mg/L) was filtered, followed by washing with distilled water for 30 minutes before allowing pure water to pass through the membrane again in the final cycle. The results of three filtration stages are presented in Fig. 8. When pure water is alternated with MB solution, the flux slightly decreases due to MB adsorption/deposition on the membrane surface. The flux measurements of MB solution are similar to those of pure water, indicating high antifouling properties. However, an increase in membrane flux may lead to a reduction in rejection due to pore size enlargement. Kesting et al. [91] have noted that increased inter-void space and loosely packed polymers result in lower reject rates in membrane filters. It is important to note that the incorporation of β-CD may alter the membrane morphology and consequently change the rejection mechanisms. With β-CD modified membranes, the separation mechanism for dyes may involve size exclusion, electrostatic interaction, and inclusion complexation [92]. A reduction in rejection rate from 94% to 66% upon adding 0.25% β-CD could be attributed to increased pore size. According to Liu [93], the mechanism of MB adsorption by β-CD involves both electrostatic interactions and inclusion complexation. As per Wang [94], MB mainly attaches to the β-CD through electrostatic attraction and π-π stacking. With a further increase of β-CD to 1%, MB rejection rates are slightly affected. The data from the last stage clearly demonstrated that the pure water flux was fully restored to the initial value for M1 (0.25 wt% bCD) membrane after membrane cleaning. We used equation (3) to calculate the FRR value to evaluate the extent of flux recovery after MB fouling, and the results, presented in Figure 9, show that a higher FRR indicates better antifouling properties. The M0 membrane had an FRR value of 91%, which increased to 100% after loading 0.25% of β-CD. However, the FRR value for M3 was the lowest, indicating only 56% recovery.

An experiment was conducted to test the effect of adding β-CD to membranes on their permeability and selectivity. To analyze the selectivity of the M1 (0.25wt% β-CD) membrane in detail, various dyes with different sizes and charges were utilized. These dyes included methylene blue (MB, positive, 0.504 nm), methyl red (MR, neutral, 0.487 nm), rose Bengal (RB, negative, 0.588 nm), and brilliant blue (BB, negative, 0.798 nm). Our study unequivocally demonstrates that the filtration process had a high rejection rate for Methyl red (MR), Rose Bengal, and Brilliant blue dyes, with rates of approximately 83%, 73%, and 99%, respectively, as shown in Figure 10. Moreover, previous research has conclusively shown that β-CD can form an inclusion complex with azo dyes like MR, which provides a plausible explanation for the high rejection rate observed for MR in our study.

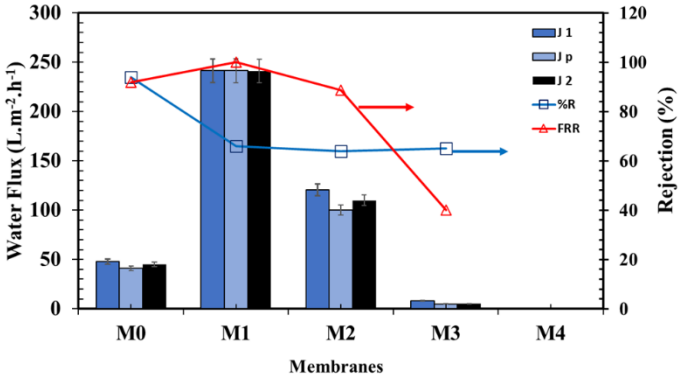

Figure 9. Water flux, Flow recovery (FRR), and Rejection of PVDF-$PVP_{(1-x)}$- β- $CD_{(x)}$ membranes **M_0** (x=0), **M_1** (x=0.25), **M_2** (x=0.50), **M_3** (x=0.75) and **M_4** (x=1.0) during MB test (J_1 = pure water flux, J_P = pollutant water flux, J_2= pure water flux after test).

 doi:10.20944/preprints202404.1247.v1

Therefore, it is likely that the formation of an inclusion complex between β-CD and MR molecules contributed to the observed result. To test this hypothesis, a new membrane was casted by substituting smaller CDs molecules like α-CD (0.47 nm) instead of βCD (0.6-0.65 nm), while keeping the loading constant at 0.25 wt%. The filtration of MR (0.478 nm) was compared among M_0, M_1 (0.25 wt% β-CD), and M_5 (0.25 wt% α-CD) membranes. The results, which can **be found in supplementary information S2,** showed that the MR rejection rate was in the order of M_2 (83%) > M_0 (27%) > M_5 (16%). This result suggests that MR might be included in the larger cage of bCD, in comparison to smaller a-CD. Otherwise, conjugated systems, like MR dyes (seven), can experience significant charge movements within their structures. This charge dislocation leads to a change in the dye's dipole moment and polarization. Since the dyes are polar, the total polarization is expected to include electronic, ionic, and dipolar polarization [95]. In this study, two dyes, MR (ε'~ 6) and MB (ε'~ 16), were compared based on their dielectric constant about the membrane pores (ε'~ 29). The two dyes used in the experiment are of similar size, which helps to avoid exclusion phenomena. However, the rejection rates of the two dyes differed: 83% for MR against 66% for MB. The difference in rejection rates can be attributed to the dielectric variance between the two dyes and the pores of the β-CD modified membrane (ε'(membrane)>> ε'(MR)). Hence, the membrane pore's unique confinement caused the dye molecules to rearrange spatially, forming distinct yet diffuse layers. This rearrangement altered the dyes' physical and electrical properties, simultaneously affecting the dielectric constant of the solution and membrane. To date, dielectric exclusion's mechanism and its variations with solute type, concentration, and number of ions on the membrane surface remain unverified. These findings provide insight into the behavior of dyes in confined spaces, which could inform future research in this area.

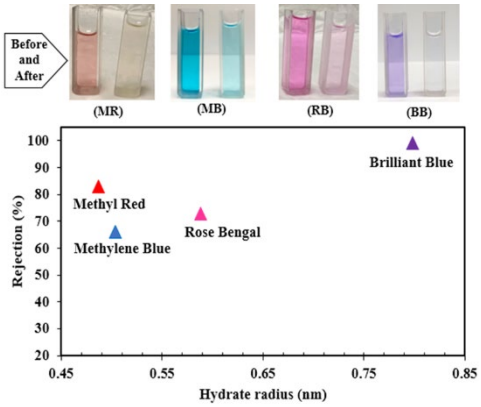

Figure 10. Rejection of different dyes by plausible dielectric exclusion (MR, MB, and RB) and size exclusion (BB) using M_1 membrane (PVDF-$PVP_{0.75}$- β- $CD_{0.25}$).

4. Conclusions

In this study, we explored the impact of adding low amounts of beta-cyclodextrin nanofillers to PVDF membrane via a simple blending method on its hydrophilicity and antifouling properties. The utilization of characterization techniques has demonstrated that the introduction of beta-cyclodextrin induces a considerable morphological transformation in the system, as evidenced by X-ray diffraction, ART-IR, SEM, and AFM. The optimized loading of β-CD has been unequivocally shown to result in a fivefold greater flux than that of a PVDF/PVP membrane, with the added advantage of the lowest resistance during the filtration process. Additionally, the introduction of bCD molecules increases the dielectric constant and conductivity of the PVDF membrane. It's important to note that a membrane's selectivity or separation power is influenced by a variety of factors, not just the size of its pores. While pore size is an important consideration, electrostatic interactions and exclusion dielectric phenomena also significantly impact. Coulomb forces resulting from the membrane's surface charge and differences in dielectric constant between the solution in the nanopores, the membrane material, and the external solution all contribute to the membrane's ability to separate dyes having different sizes and charges selectively. When smaller cages of aCD are used instead of

 doi:10.20944/preprints202404.1247.v1

bCD, the inclusion of dye is no longer possible. By understanding and optimizing these factors, we can develop membranes with improved selectivity and separation efficiency.

Supplementary Materials: The following supporting information can be downloaded at: www.mdpi.com/xxx/s1, Figure S1: Membrane resistance of PVDF-PVP$_{(1-x)}$- β- CD$_{(x)}$ membranes: M$_0$ (x=0), M$_1$ (x=0.25), M$_2$ (x=0.50), M$_3$ (x=0.75) and M$_4$ (x=1.0).; Figure S2: Methyl Red (MR) rejection with different membranes: **M$_5$** (PVDF-PVP $_{(0.75)}$- a-CD$_{(0.25)}$), **M$_0$** (PVDF-PVP), and **M$_1$** (PVDF-PVP $_{(0.75)}$- bCD$_{(0.25)}$).

Author Contributions: "Conceptualization, W.R. and H.K.; methodology, W.R. and H.K.; software, H.K.; validation, W.R, H.K. and I.E.; formal analysis, H.K.; investigation, H.K.; resources, H.K.; data curation, H.K; writing—original draft preparation, W.R; writing—review and editing, H.K; visualization, H.K.; supervision, H.K.; project administration, H.K.; funding acquisition, H.K. All authors have read and agreed to the published version of the manuscript.".

Funding: The authors would like to acknowledge the funding from Ministry of Education (IF-2020-018-BASRC) and Imam Abdulrahman Bin Faisal University, Basic and Applied Scientific Research Center for their support.

Conflicts of Interest: Declare conflicts of interest or state "The authors declare no conflicts of interest.".

References

1. N. Salim, A. Siddiqa, S. Shahida, and S. Qaisar. PVDF based Nanocomposite Membranes: Application towards Wastewater treatment. *Madridge J Nanotechnol Nanosci.*, **2019**, 4, 139–147. doi: https://doi.org/10.18689/mjnn-1000128.
2. S. Kalogirou, Seawater desalination using renewable energy sources. *Prog. Energy Combust. Sci.,* **2005**, *31*, 242–281. doi: https://doi.org/10.1016/j.pecs.2005.03.001.
3. N. L. Le and S. P. Nunes. Materials and membrane technologies for water and energy sustainability. *Sustain Mater Techno.*, **2016**, 7, 1–28. doi: https://doi.org/10.1016/j.susmat.2016.02.001.
4. C. Okello, B. Tomasello, N. Greggio, N. Wambiji, and M. Antonellini. Impact of Population Growth and Climate Change on the Freshwater Resources of Lamu Island, Kenya. *Water*, **2015**, *7*, 1264–1290. doi: https://doi.org/10.3390/w7031264.
5. M. K. Daud, M. Nafees, S. Ali, M. Rizwan, R. Ahmad Bajwa, M.B.Shakoor, M. Umair Arshad, S. Ali Shahid Chatha, F.Deeba, W. Murad, F. Malook, S. J. Zhu. Drinking Water Quality Status and Contamination in Pakistan. *Int. J. Biomed. Res,* **2017**, 2017, 1–18. doi: https://doi.org/10.1155/2017/7908183.
6. M. M. Iqbal, M. Imran, T. Hussain, M. Asif Naeem , A. A. Al-Kahtani, **G.** M. Shah , S. Ahmad, A. Farooq, M. Rizwan, A. Majeed, A. Rehman Khan, S. Ali. Effective sequestration of Congo red dye with ZnO/cotton stalks biochar nanocomposite: MODELING, reusability and stability. *J. Saudi Chem. Soc.*, **2021**, *25*, 101176. doi: https://doi.org/10.1016/j.jscs.2020.101176.
7. M. Mao, T. Yan, J. Shen, J. Zhang, and D. Zhang. Capacitive Removal of Heavy Metal Ions from Wastewater via an Electro-Adsorption and Electro-Reaction Coupling Process. *Environ. Sci. Technol*, **2021**, *55*, 3333–3340. doi: https://doi.org/10.1021/acs.est.0c07849.
8. T. Haneef, B. Nur Karahan, Y. Akdag, M. Fakioglu, S. Korkut, H. Guven, M.E. Ersahin, H. Ozgun. Removal of Polycyclic Aromatic Hydrocarbons (PAHs) from Produced Water by Ferrate (VI) Oxidation. *Water*, **2020**, *12*, 3132. doi: https://doi.org/10.3390/w12113132.
9. B. Nur Karahan, Y. Akdag, M. Fakioglu , S. Korkut , Huseyin Guven [a], Mustafa E. Ersahin , H. Ozgun . Coupling ozonation with hydrogen peroxide and chemically enhanced primary treatment for advanced treatment of grey water. *J. Environ. Chem. Eng.*, **2023**, *11*, 110116–110116. doi: https://doi.org/10.1016/j.jece.2023.110116.
10. D. Cristina, P. Chelme-Ayala, and Mohamed Gamal El-Din. Sludge-based activated biochar for adsorption treatment of real oil sands process water: Selectivity of naphthenic acids, reusability of spent biochar, leaching potential, and acute toxicity removal.*J. Chem. Eng,* **2023**, *463*, 142329–142329. doi: https://doi.org/10.1016/j.cej.2023.142329.
11. W.Alrashedi,H. Kochkar, G. Berhault , M. Younas , A. Ali, N.A. Alomair, R. Hamdi , S.A. Abubshait , O. Alagha , M.F. Gondal , M. Haroun , C. Tratrat. Enhancement of the photocatalytic response of Cu-doped TiO2 nanotubes induced by the addition of strontium. *J. Photochem. Photobiol., A*, **2022**, *428*, 113858–113858. doi: https://doi.org/10.1016/j.jphotochem.2022.113858.
12. A. Oulkhir, K. Lyamlouli, M. Danouche, and R. Benhida. Biosorption of a cationic dye using raw and functionalized Chenopodium quinoa pericarp biomass after saponin glycosides extraction. *J. Environ. Chem. Eng.*, **2023**, *11*, 110419–110419. doi: https://doi.org/10.1016/j.jece.2023.110419.
13. Da Li , X. Zhang , X. Liang , W. Liu, K. Guo, Z. Zhang, S. Wang, Y. Xing, Z. Li, J. Li , H. Wang. Simultaneous removal and conversion of silver ions from wastewater into antibacterial material through

selective chemical precipitation. *Arab. J. Chem.*, **2023**, *16*, 104836–104836. doi: https://doi.org/10.1016/j.arabjc.2023.104836.

14. E. F. Aboelfetoh, A. E. Aboubaraka, and E.-Z. M. Ebeid. Binary coagulation system (graphene oxide/chitosan) for polluted surface water treatment," Environ. Manag., **2021**, *288*, 112481. doi: https://doi.org/10.1016/j.jenvman.2021.112481.
15. Y. Dong, H. Wu, F. Yang, and S. Gray. Cost and efficiency perspectives of ceramic membranes for water treatment. *Water Res.*, **2022**, 220, 118629. doi: https://doi.org/10.1016/j.watres.2022.118629.
16. K.Zuo, K. Wang, R.M. DuChanois, Q. Fang, E.M. Deemer, X.Huang, R. Xin, I.,A. Said, Z.He, Y. Feng , W. Shane Walker, J. Lou , M. Elimelech, , Q. Li . Selective membranes in water and wastewater treatment: Role of advanced materials. *Mater.Today*, **2021**, *50*, 516-532 doi: https://doi.org/10.1016/j.mattod.2021.06.013.
17. Z. He, Y. Li, G. Liu, C. Wang, S. Chang, J. Hu , X. Zhang, Y .Vasseghian. Fabrication of a novel hollow wood fiber membrane decorated with halloysite and metal-organic frameworks nanoparticles for sustainable water treatment. *Ind. Crops and Products*, **2023**, *202*, 117082–117082. doi: https://doi.org/10.1016/j.indcrop.2023.117082.
18. M. Daramola, E. Aransiola, and T. Ojumu. Potential Applications of Zeolite Membranes in Reaction Coupling Separation Processes. *Mater.*, **2012**, *5*, 2101–2136. doi: https://doi.org/10.3390/ma5112101.
19. A. S. Mohammed, M. Soliman, S. Kandil, S. Ebrahim, and M. Khalil. Tailoring nanocomposite membranes of cellulose acetate/silica nanoparticles for desalination. J. Materiomics, **2022**, *8*, 1122–1130. doi: https://doi.org/10.1016/j.jmat.2022.07.001.
20. T. Guo-quan, L. Shengzhe, H. Yuxiao , L. Zhuo , L. Jie , L. Xin , L. Weiyi. Fabrication of chitosan membranes via aqueous phase separation: Comparing the use of acidic and alkaline dope solutions. *J. Membr. Sci.*, **2022**, *646*, 120256–120256. doi: https://doi.org/10.1016/j.memsci.2022.120256.
21. H. Wei, R. Chen, and G. Li. Effect of chemical structure on the performance of sulfonated poly (arylene ether sulfone) as proton exchange membrane. *Int. J. Hydrogen Energy*. **2015**, *40*, 14392–14397 doi: https://doi.org/10.1016/j.ijhydene.2015.03.087.
22. M. Kwong, A. Abdelrasoul, and H. Doan. Controlling polysulfone (PSF) fiber diameter and membrane morphology for an enhanced ultrafiltration performance using heat treatment. *Results Mater*, **2019**, *2*, 100021. doi: https://doi.org/10.1016/j.rinma.2019.100021.
23. M. Amid, N. Nabian, and M. Delavar. Fabrication of polycarbonate ultrafiltration mixed matrix membranes including modified halloysite nanotubes and graphene oxide nanosheets for olive oil/water emulsion separation. *Sep. Pur. Tech.*, **2020**, *251*, 117332. doi: https://doi.org/10.1016/j.seppur.2020.117332.
24. Z. Wu, X. Ji, Q. He, H. Gu, W. Zhang, and Z. Deng. Nanocelluloses fine-tuned polyvinylidene fluoride (PVDF) membrane for enhanced separation and antifouling. *Carbohydr. Polym*, **2024**, *323*, 121383–121383. doi: https://doi.org/10.1016/j.carbpol.2023.121383.
25. A. N. Arshad, M. H. M. Wahid, M. Rusop, W. H. A. Majid, R. H. Y. Subban, and M. D. Rozana. Dielectric and Structural Properties of Poly(vinylidene fluoride) (PVDF) and Poly(vinylidene fluoride-trifluoroethylene) (PVDF-TrFE) Filled with Magnesium Oxide Nanofillers. *J. Nanomater.*, **2019**, *2019*, 1–12. doi: https://doi.org/10.1155/2019/5961563.
26. C. Guo, S. Haiting, W. Wei , P. Xiaoyuan , T. Kunyue, H. Yanli, X. Zhiwei, D. Hui , Q. Xiaoming. Improvement of PVDF nanofiltration membrane potential, separation and anti-fouling performance by electret treatment. *Sci. Total Environ.*, **2020**, *722*, 137816–137816. doi: https://doi.org/10.1016/j.scitotenv.2020.137816.
27. M. Li, I. Katsouras, C. Piliego, G. Glasser, I. Lieberwirth, P. W. M. Blomb , D..M. de Leeuw. Controlling the microstructure of poly(vinylidene-fluoride) (PVDF) thin films for microelectronics. *J. Mater. Chem. C*, **2013**, *1*, 7695, 2013. doi: https://doi.org/10.1039/c3tc31774a.
28. X. Wang, D. Chen, T. He, Y.Zhou, L. Tian, Z. Wang, Z. Cui. Preparation of Lateral Flow PVDF Membrane via Combined Vapor- and Non-Solvent-Induced Phase Separation (V-NIPS). *Membr. J.*, **2023**, *13*, 91–91. doi: https://doi.org/10.3390/membranes13010091.
29. M. Amini, S. A. Haddadi, S. Ghaderi, A. Ramazani, and Mohammad Hassan Ansarizadeh. Preparation and characterization of PVDF/Starch nanocomposite nanofibers using electrospinning method. ***Mater. Today Proc***, **2018**, *5*, 15613–15619. doi: https://doi.org/10.1016/j.matpr.2018.04.170.
30. J.Zhang, Y. Yang,Z. Sun, D. Zhao, Y. Gao, T. Shen, Y. Li, Z. Xie, Y.Huo, H. Li. Ag@BiOBr/PVDF photocatalytic membrane for remarkable BSA anti-fouling performance and insight of mechanism. *J. Membr. Sci.*, **2023**, *677*, 121611–121611. doi: https://doi.org/10.1016/j.memsci.2023.121611.
31. J. Jiang, B. Ma, C. Yang, X. Duan, and Q. Tang. Fabrication of anti-fouling and photo-cleaning PVDF microfiltration membranes embedded with N-TiO_2 photocatalysts. *Sep. Purif. Technol.*, **2022**, *298*, 121673. doi: https://doi.org/10.1016/j.seppur.2022.121673.
32. L. Lik, C. C. Chou, and J. Chen. Hybrid model based expected improvement control for cyclical operation of membrane microfiltration processes. *Chem. Eng. Sci*, **2017**, *166*, 77–90. doi: https://doi.org/10.1016/j.ces.2017.02.048.

33. W. Sun, J. Liu, H. Chu, and B. Dong. Pretreatment and Membrane Hydrophilic Modification to Reduce Membrane Fouling. *Membranes*, **2013**, *3*, 226–241. doi: https://doi.org/10.3390/membranes3030226.
34. S. Zhang, L. Wu, F. Deng, D. Zhao, C. Zhang, and C. Zhang. Hydrophilic modification of PVDF porous membrane via a simple dip-coating method in plant tannin solution. *RSC Adv.*, **2016**, *6*, 71287–71294. doi: https://doi.org/10.1039/c6ra13634f.
35. W. Xie, J. Li, T. Sun, W. Shang, W. Dong, M. Li, F. Sun. Hydrophilic modification and anti-fouling properties of PVDF membrane via in situ nano-particle blending. *Environ. Sci. Pollut. Res.*, **2018**, *25*, 25227–25242. doi: https://doi.org/10.1007/s11356-018-2613-y.
36. X. Meng, Y. Ji, G. Yu, and Y. Zhai. Preparation and Properties of Polyvinylidene Fluoride Nanocomposite Membranes based on Poly(N-Isopropylacrylamide) Modified Graphene Oxide Nanosheets. *Polym.*, **2019**, *11*, 473. doi: https://doi.org/10.3390/polym11030473.
37. R. Gayatri, A. N. Syimir Fizal, E. Yuliwati, S. Hossain, J. Jaafar, M. Zulkifli, W. Taweepreda, A. Naim Ahmad Yahaya. Preparation and Characterization of PVDF–TiO2 Mixed-Matrix Membrane with PVP and PEG as Pore-Forming Agents for BSA Rejection. *Nanomater.*, **2023**, *13*, 1023–1023. doi: https://doi.org/10.3390/nano13061023.
38. O. A. Koriem, M. S. Showman, A.H. El-Shazly, and M.F. Elkady. Cellulose acetate/polyvinylidene fluoride based mixed matrix membranes impregnated with UiO-66 nano-MOF for reverse osmosis desalination. *Cellulose*, **2022**, *30*, 413–426. doi: https://doi.org/10.1007/s10570-022-04889-9.
39. R. Pang, L. Xin, L. Jian-Sheng, L. Zhuang-Yu, H. Cheng, S. Xiu-Yun, W. Lian-Jun. In situ Preparation and Antifouling Performance of ZrO2/PVDF Hybrid Membrane. *Acta Phys. -Chim. Sin.*, **2013**, *29*, 2592–2598. doi: https://doi.org/10.3866/pku.whxb201310291.
40. X. Yue, X. Ji, H. Xu, B. Yang, M. Wang, and Y. Yang. Performance investigation on GO-TiO2/PVDF composite ultrafiltration membrane for slightly polluted groundwater treatment. *Energy*, **2023**, *273*, 127215. doi: https://doi.org/10.1016/j.energy.2023.127215.
41. N. Alnairat, M. Abu Dalo, R. Abu-Zurayk, S. Abu Mallouh, F. Odeh, and A. Al Bawab. Green Synthesis of Silver Nanoparticles as an Effective Antibiofouling Material for Polyvinylidene Fluoride (PVDF) Ultrafiltration Membrane. *Polymers*, **2021**, *13*, 3683. doi: https://doi.org/10.3390/polym13213683.
42. C. Chen, Q. Liu, W. Chen, F. Li, G. Xiao, C. Chen, R. Li, J. Zhou. A high absorbent PVDF composite membrane based on β-cyclodextrin and ZIF-8 for rapid removing of heavy metal ions. Separation and Purification Technology, **2022**, 292, 120993–120993. doi: https://doi.org/10.1016/j.seppur.2022.120993.
43. J.-F. Li, Z.-L. Xu, H. Yang, L.-Y. Yu, and M. Liu. Effect of TiO2 nanoparticles on the surface morphology and performance of microporous PES membrane. *Appl. Surf. Sci.*, **2009**, *255*, 4725–4732. doi: https://doi.org/10.1016/j.apsusc.2008.07.139.
44. R. Roshani, F. Ardeshiri, M. Peyravi, and M. Jahanshahi. Highly permeable PVDF membrane with PS/ZnO nanocomposite incorporated for distillation process. *RSC Adv.*, **2018**, *8*, 23499–23515. doi: https://doi.org/10.1039/c8ra02908c.
45. X. Cao, J. Ma, X. Shi, and Z. Ren. Effect of TiO2 nanoparticle size on the performance of PVDF membrane. *Appl. Surf. Sci.*, **2006**, *253*, 2003–2010. doi: https://doi.org/10.1016/j.apsusc.2006.03.090.
46. F. Ardeshiri, S. Salehi, M. Peyravi, M. Jahanshahi, A. Amiri, and A. Shokuhi Rad. PVDF membrane assisted by modified hydrophobic ZnO nanoparticle for membrane distillation. *Asia-Pac. J. Chem. Eng.*, **2018**, *13*. doi: https://doi.org/10.1002/apj.2196.
47. M. Jiang, R. Simayi, Amatjan Sawut, J. Wang, T. Wu, and X. Gong. Modified β-Cyclodextrin hydrogel for selective adsorption and desorption for cationic dyes. *Coll. Surf. Colloid Surf. Physicochem. Eng. Asp*, **2023**, *661*, 130912–130912. doi: https://doi.org/10.1016/j.colsurfa.2022.130912.
48. H. Yamasaki, Aya Odamura, Yousuke Makihata, and K. Fukunaga. Preparation of new photo-crosslinked β-cyclodextrin polymer beads. *Polymer J.*, **2017**, *49*, 377–383. doi: https://doi.org/10.1038/pj.2016.127.
49. S. Pereva, V. Nikolova, S. Angelova, T. Spassov, and T. Dudev. Water inside β-cyclodextrin cavity: Amount, stability and mechanism of binding. *Beilstein J. Org. Chem.*, **2019**, *15*, 1592–1600. doi: https://doi.org/10.3762/bjoc.15.163.
50. J. Xue, J. Shen, R. Zhang, F.Wang, S. Liang, X. You, Q. Yu, Y. Hao, Y. Su, Z. Jiang. High-flux nanofiltration membranes prepared with β-cyclodextrin and graphene quantum dots. *J. Membr. Sci.*, **2020**, *612*, 118465–118465. doi: https://doi.org/10.1016/j.memsci.2020.118465.
51. A. Mohammadi and P. Veisi. High adsorption performance of β-cyclodextrin-functionalized multi-walled carbon nanotubes for the removal of organic dyes from water and industrial wastewater. *J. Environ. Chem. Eng.*, **2018**, 6, 4634–4643. doi: https://doi.org/10.1016/j.jece.2018.07.002.
52. J.C. Lee, S. L.Hulu, C. H. Park, C. S. Kim. Enhancing the anti-bacterial activity of nanofibrous polyurethane membranes by incorporating glycyrrhizic acid-conjugated β-Cyclodextrin. *Mater. Lett.*, **2023**, *338*, 134030–134030. doi: https://doi.org/10.1016/j.matlet.2023.134030.
53. Y. Lv, J. Ma, K. Liu, Y. Jiang, G. Yang, Y. Liu, C. Lin, X. Ye, Y. Shi, M. Liu, L. Chen. Rapid elimination of trace bisphenol pollutants with porous β-cyclodextrin modified cellulose nanofibrous membrane in water:

Adsorption behavior and mechanism. J. *Hazard. Mater.*, **2021**, *403*, 123666–123666. doi: https://doi.org/10.1016/j.jhazmat.2020.123666.

54. Z. Yang, X. Liu, X. Liu, J. Wu, X. Zhu, Z. Bai, Z. Yu. Preparation of β-cyclodextrin/graphene oxide and its adsorption properties for methylene blue. *Colloids Surfaces B.*, **2021**, *200*, *1*11605–111605. doi: https://doi.org/10.1016/j.colsurfb.2021.111605.
55. S. Janakiraman, A. Surendran, S. Ghosh, S. Anandhan, and A. Venimadhav. Electroactive poly(vinylidene fluoride) fluoride separator for sodium ion battery with high coulombic efficiency. *Solid State Ion.*, **2016**, *292*, 130–135. doi: https://doi.org/10.1016/j.ssi.2016.05.020.
56. T. Wu, B. Zhou, T. Zhu, J. Shi, Z. Xu, C. Hua, J. Wang. Facile and low-cost approach towards a PVDF ultrafiltration membrane with enhanced hydrophilicity and antifouling performance via graphene oxide/water-bath coagulation. *RSC Adv.*, **2015**, *5*, 7880–7889. doi: https://doi.org/10.1039/c4ra13476a.
57. Pradeep Kumar Mahato, A. K. Seal, Samiran Garain, and S. Sen. Effect of fabrication technique on the crystalline phase and electrical properties of PVDF films. *Mater. Sci.-Pol.*, **2015**, *33*, 157–162. doi: https://doi.org/10.1515/msp-2015-0020.
58. A. Popa, D. Toloman, M. Stan, M. Stefan, T. Radu, G. Vlad, S. Ulinici, G. Baisan, S. Macavei, L. Barbu-Tudoran, O. Pana. Tailoring the RhB removal rate by modifying the PVDF membrane surface through ZnO particles deposition. *J.Inorg. Organomet. Polym.*, **2021**, *31*, 1642–1652. doi: https://doi.org/10.1007/s10904-020-01795-0.
59. P. Singh, H. Borkar, B. P. Singh, V. N. Singh, and A. Kumar. Ferroelectric polymer-ceramic composite thick films for energy storage applications. *AIP Adv.*, **2014**, *4*, 087117. doi: https://doi.org/10.1063/1.4892961.
60. Y. Zhang, J. Kang, J. Y. Chen, Y. Cao, and M. Xiang. Crystallization behavior, tensile behavior and hydrophilicity of poly(vinylidene fluoride)/poly(vinyl pyrrolidone) blends. *Polym. Sci. Ser.A*, **2014**, *56*, 864–873. doi: https://doi.org/10.1134/s0965545x14060212.
61. B. Eren, E. Eren, M. Guney, Y.C. Jean, and J.Van Horn. Positron annihilation lifetime spectroscopy study of polyvinylpyrrolidone added polyvinylidene fluoride membranes: Investigation of free volume and permeation relationships. *J. of Polym. Sci.*, **2020**, *58*. doi: https://doi.org:10.1002/pol.20190031.
62. H. Bai, X. Wang, Y. Zhou, and L. Zhang. Preparation and characterization of poly(vinylidene fluoride) composite membranes blended with nano-crystalline cellulose. *Prog. Nat. Sci.: Mater. Int.*, **2012**, *22*, 250–257. doi: https://doi.org/10.1016/j.pnsc.2012.04.011.72.
63. M. Kamaz, A. Sengupta, A. Gutierrez, Y.-H. Chiao, and R. Wickramasinghe. Surface Modification of PVDF Membranes for Treating Produced Waters by Direct Contact Membrane Distillation. *IJERPH*, **2019**, *16*, 685. doi: https://doi.org/10.3390/ijerph16050685.
64. S. Kartohardjono, G. M. Salsabila, A. Ramadhani, I. Purnawan, and W. Jye Lau. Preparation of PVDF-PVP Composite Membranes for Oily Wastewater Treatment. *Membranes*, **2023**, *13*, 611. doi: https://doi.org/10.3390/membranes13060611.
65. H. M. Zidan, E.M. Abdelrazek, A.M. Abdelghany, and A. E. Tarabiah. Characterization and some physical studies of PVA/PVP filled with MWCNTs. *JMST*, **2019**, *8*, 904–913. doi: https://doi.org/10.1016/j.jmrt.2018.04.023.
66. H. Rachmawati, C. A. Edityaningrum, and R. Mauludin. Molecular Inclusion Complex of Curcumin–β-Cyclodextrin Nanoparticle to Enhance Curcumin Skin Permeability from Hydrophilic Matrix Gel. *AAPS Pharm. Sci. Tech*, **2013**, *14*, 1303–1312. doi: https://doi.org/10.1208/s12249-013-0023-5.
67. R. L. Abarca, F. J. Rodríguez, A. Guarda, M. J. Galotto, and J. E. Bruna. Characterization of beta-cyclodextrin inclusion complexes containing an essential oil component. *Food Chem.*, **2016**, *196*, 968–975. doi: https://doi.org/10.1016/j.foodchem.2015.10.023.
68. I. Tijunelyte, N. Dupont, I. Milosevic, C. Barbey, E. Rinnert, N. Lidgi-Guigui, E. Guenin, M. Lamy de la Chapelle. Investigation of aromatic hydrocarbon inclusion into cyclodextrins by Raman spectroscopy and thermal analysis. *Environ. Sci. Pollut. Res.*, **2017**, *24*, 27077–27089. https://doi.org/10.1007/s11356-015-4361-6.
69. M. McNamara, N. R. Russell. FT-IR and Raman Spectra of a Series of Metallo-Cyclodextrin Complexes. J. Incl. Phenom. and Molec. Reco & Chem., **1991**, *10*, 485–495.
70. A. C. D. Morihama and J. C. Mierzwa. Clay nanoparticles effects on performance and morphology of poly(vinylidene fluoride) membranes. *Braz. J. Chem. Eng.*, **2014**, *31*, 79–93. doi: https://doi.org/10.1590/s0104-66322014000100009.
71. A. C. Sun, W. Kosar, Y. Zhang, and X. Feng. A study of thermodynamics and kinetics pertinent to formation of PVDF membranes by phase inversion. *Desalination*, **2013**, *309*, 156–164. doi: https://doi.org/10.1016/j.desal.2012.10.005.
72. C. Bărdacă Urducea, A. C. Nechifor, I. A. Dimulescu, O. Oprea, G. Nechifor, E. Eftimie Totu, I. Isildak, P. C. Albu, S. G. Bungău. Control of Nanostructured Polysulfone Membrane Preparation by Phase Inversion Method. *Nanomaterials*, **2020**, 10, 2349. doi: https://doi.org/10.3390/nano10122349.
73. W. Lu, Z. Yuan, Y. Zhao, H. Zhang, H. Zhang, and X. Li. Porous membranes in secondary battery technologies. *Chem. Soc. Rev.*, **2017**, *46*, 2199–2236. doi: https://doi.org/10.1039/c6cs00823b.

74. H.-T. Yeo, S.-T. Lee, and M. Han. Role of a Polymer Additive in Casting Solution in Preparation of Phase Inversion Polysulfone Membranes. *JCEJ*, **2000**, 33, 180–184. https://doi.org/10.1252/jcej.33.180.
75. X. Liu, H. Yuan, C. Wang, S. Zhang, L. Zhang, X. Liu, F. Liu, X. Zhu, S.Rohani, C. Ching, J. Lu. A novel PVDF/PFSA-g-GO ultrafiltration membrane with enhanced permeation and antifouling performances. *Sep. Pur. Tech.* **2020**, *233*, 116038–116038. doi: https://doi.org/10.1016/j.seppur.2019.116038.
76. M. Safarpour, A. Khataee, and V. Vatanpour. Preparation of a Novel Polyvinylidene Fluoride (PVDF) Ultrafiltration Membrane Modified with Reduced Graphene Oxide/Titanium Dioxide (TiO2) Nanocomposite with Enhanced Hydrophilicity and Antifouling Properties. *Ind. Eng. Chem. Res.*, **2014**, *53*, 13370–13382. doi: https://doi.org/10.1021/ie502407g.
77. B. Vatsha, J. C. Ngila, and R. M. Moutloali. Preparation of antifouling polyvinylpyrrolidone (PVP 40K) modified polyethersulfone (PES) ultrafiltration (UF) membrane for water purification. *Physics and Chemistry of the Earth, Parts A/B/C*, **2014**, *67–69*, 125–131. doi: https://doi.org/10.1016/j.pce.2013.09.021.
78. M. Baghbanzadeh, D. Rana, T. Matsuura, and C. Q. Lan. Effects of hydrophilic CuO nanoparticles on properties and performance of PVDF VMD membranes. *Desalination*, **2015**, *369*, 75–84. doi: https://doi.org/10.1016/j.desal.2015.04.032.
79. M. S. Rameetse, O. Aberefa, and M. O. Daramola. Effect of Loading and Functionalization of Carbon Nanotube on the Performance of Blended Polysulfone/Polyethersulfone Membrane during Treatment of Wastewater Containing Phenol and Benzene. *Membranes*, **2020**, *10*, 54. doi: https://doi.org/10.3390/membranes10030054.
80. Y. Du, P. Yang, Z. Mou, Hua Nan-ping, and L. Jiang. Thermal decomposition behaviors of PVP coated on platinum nanoparticles. *J. Appl. Polym. Sci.*, **2005**, *99*, 23–26. doi: https://doi.org/10.1002/app.21886.
81. S. F. Mohamad, M. I. Mustaqim Azzian, N. M. Hakimi, M. Abdul Manaf, D. Ramesh, T. Asogan, N.H. Ismail, W. Salleh, Physicochemical properties of poly (vinylidene fluoride) membrane grafted poly hydroxyethyl acrylates using radiation-induced graft admicellar polymerization. *Mater. Tod. Proceedings*, **2023**, ISSN 2214-7853, https://doi.org/10.1016/j.matpr.2023.02.010.
82. Z. Yu, Y. Pan, Y. He, G. Zeng, H. Shi, and H. Di. Preparation of a novel anti-fouling β-cyclodextrin–PVDF membrane. *RSC Adv.*, **2015**, *5*, 51364–51370. doi: https://doi.org/10.1039/c5ra04894j.
83. Y. Lu, Y. Ma, T. Yang, and J. Guo. Hydrophilic modification of PVDF membranes by in situ synthesis of nano-Ag with nano-ZrO_2. *Green Process. Synth.*, **2021**,*10*, 538–546. doi: https://doi.org/10.1515/gps-2021-0050.
84. A. Karimi, A. Khataee, A. Ghadimi, and V. Vatanpour. Ball-milled Cu2S nanoparticles as an efficient additive for modification of the PVDF ultrafiltration membranes: Application to separation of protein and dyes. *J. Environ. Chem. Eng.*, **2021**, *9*, 105115. doi: https://doi.org/10.1016/j.jece.2021.105115.
85. J. Li, X. Liu, J. Lu, Yudan Chen Wang, G. Li, and L. Liu. Anti-bacterial properties of ultrafiltration membrane modified by graphene oxide with nano-silver particles. *J. Colloid Interface Sci.* **2016**, *484*, 107–115. doi: https://doi.org/10.1016/j.jcis.2016.08.063.
86. J. Ma, Y. He, G. Zeng, X.Yang, X. Chen, L. Zhou, L. Peng, A. Sengupta. High-flux PVDF membrane incorporated with β-cyclodextrin modified halloysite nanotubes for dye rejection and Cu (II) removal from water. *Polym. Adv. Technol.*, **2018**, *29*, 2704–2714. doi: https://doi.org/10.1002/pat.4356.
87. E. Abdollahi, A. Heidari, T. Mohammadi, A. Asadi, and Maryam Ahmadzadeh Tofighy. Application of Mg-Al LDH nanoparticles to enhance flux, hydrophilicity and antifouling properties of PVDF ultrafiltration membrane: Experimental and modeling studies. *Sep. Purif. Technol.*, **2021**, *257*, 117931–117931. doi: https://doi.org/10.1016/j.seppur.2020.117931.
88. H. Nawaz, M. Umar, I. Nawaz, Q. Zia, M. Tabassum, H, Razzaq, H. Gong, X. Zhao, X. Liu. Photodegradation of textile pollutants by nanocomposite membranes of polyvinylidene fluoride integrated with polyaniline–titanium dioxide nanotubes. *J. Chem. Eng*, **2021**, *419*, 129542. doi: https://doi.org/10.1016/j.cej.2021.129542.
89. H. Srivastava, G. Arthanareeswaran, N. Anantharaman, V. Starov. Performance of modified poly(vinylidene fluoride) membrane for textile wastewater ultrafiltration. *Desalination*, **2011**, *282*, 87–94. doi: https://doi.org/10.1016/j.desal.2011.05.054.
90. H, Dalong, Y, Wang, S, Song, S, Liu, Y, Deng. Significantly Enhanced Dielectric Performances and High Thermal Conductivity in Poly(vinylidene fluoride)- Based Composites Enabled by SiC@SiO2 Core–Shell Whiskers Alignment. *ACS Appl. Mater. Interfaces*. **2017**, *51*, 44839–44846.
91. R. E. Kesting, Synthetic polymeric membranes: A structural perspective. New York: Wiley, 1985.
92. X. Li, L. Xie, X. Yang, and X. Nie. Adsorption behavior and mechanism of β-cyclodextrin–styrene-based polymer for cationic dyes. *RSC Adv*. **2018**, *8*, 40321–40329. doi: https://doi.org/10.1039/c8ra07709f.
93. J. Liu, G. Liu, W. Liu. Preparation of water-soluble β-cyclodextrin/poly(acrylic acid)/graphene oxide nanocomposites as new adsorbents to remove cationic dyes from aqueous solutions. *J. Chem. Eng*, **2014**, 257, *299–308*. doi https://doi.org/10.1016/j.cej.2014.07.021.

 doi:10.20944/preprints202404.1247.v1

94. J. Wang, L. Dai, Y. Liu , R. Li, X. Yang, G. Lan, H. Qiu, B. Xu. Adsorption properties of β-cyclodextrin modified hydrogel for methylene blue. *Carbohydr. Res.*, **2021**, *501*, 108276–108276. doi: https://doi.org/10.1016/j.carres.2021.108276.
95. V R K. Murthy, T.A. Prasada Rao, J. Sobhanadri. Dielectric properties of some dyes in the radio-frequency region. *J. Phys. D: Appl. Phys.*, **1977**, *10*, 2405–2409.